Title

Small scale membrane mechanics

Journal

Biomechanics and Modeling in Mechanobiology, 13(4)

ISSN

1617-7959

Authors

Rangamani, Padmini

Benjamini, Ayelet

Agrawal, Ashutosh

et al.

Publication Date

2014-08-01

DOI

10.1007/s10237-013-0528-6

Peer reviewed

Published in final edited form as:
Biomech Model Mechanobiol. 2014 August ; 13(4): 697–711. doi:10.1007/s10237-013-0528-6.

Small scale membrane mechanics

Padmini Rangamani,
Department of Molecular and Cellular Biology, University of California, Berkeley, CA 94720, USA

Ayelet Benjamini,
Department of Chemistry, University of California, Berkeley, CA 94720, USA

Ashutosh Agrawal,
Department of Mechanical Engineering, University of Houston, Houston, TX 77204, USA

Berend Smit,
Department of Chemical and Biomolecular Engineering and Department of Chemistry, University of California, Berkeley, CA 94720, USA. Materials Sciences Division, Lawrence Berkeley National Laboratory, Berkeley, CA 94720, USA

David J. Steigmann, and
Department of Mechanical Engineering, University of California, Berkeley, CA 94720, USA

George Oster
Department of Molecular and Cellular Biology, University of California, Berkeley, CA 94720, USA

David J. Steigmann: steigman@me.berkeley.edu; George Oster: goster@berkeley.edu

Abstract

Large scale changes to lipid bilayer shapes are well represented by the Helfrich model. However, there are membrane processes that take place at smaller length scales that this model cannot address. In this work, we present a one-dimensional continuum model that captures the mechanics of the lipid bilayer membrane at the length scale of the lipids themselves. The model is developed using the Cosserat theory of surfaces with lipid orientation, or 'tilt', as the fundamental degree of freedom. The Helfrich model can be recovered as a special case when the curvatures are small and the lipid tilt is everywhere zero. We use the tilt model to study local membrane deformations in response to a protein inclusion. Parameter estimates and boundary conditions are obtained from a coarse-grained molecular model using dissipative particle dynamics (DPD) to capture the same phenomenon. The continuum model is able to reproduce the membrane bending, stretch and lipid tilt as seen in the DPD model. The lipid tilt angle relaxes to the bulk tilt angle within 5–6 nm from the protein inclusion. Importantly, for large tilt gradients induced by the proteins, the tilt energy contribution is larger than the bending energy contribution. Thus, the continuum model of tilt accurately captures behaviors at length scales shorter than the membrane thickness.

Correspondence to: David J. Steigmann, steigman@me.berkeley.edu.

Keywords

Membranes; Lipid bilayers; Curvature; Mathematical model

1 Introduction

Continuum models of bilayer membranes are used to study the deformation of membranes and to explain many biological phenomena. The most popular model of lipid bilayers is the Helfrich model (Helfrich 1973), where the energy per unit area of the membrane depends only on the mean and Gaussian curvatures of the membrane. This model has been widely used to study the shape of red blood cells (Iglic 1997; Deuling and Helfrich 1976; Lim et al. 2002) and to explain biological phenomena such as the formation of membrane tubes (Derényi et al. 2002) and the shapes of lipid vesicles (Seifert et al. 1991, 1996; Jaric et al. 1995; Nelson et al. 1995). The Helfrich model assumes that the lipids are aligned normal to the membrane surface at all times and that curvatures are of the order of the bilayer thermal wavelength (~20 nm). This approach captures the changes in membrane shape that occur at large length scales.

When the membrane has lipids of different length, all of which are still aligned normal to the membrane surface, the variation in thickness can be addressed by the ‘mattress’ model (Bloom and Mouritsen 1984) to explain the variation in thickness of the membrane. More recently, Bitbol et al. (2012) have shown that the thickness gradient in the membrane observed in nanoscale studies can be explained by keeping the terms in the Hamiltonian involving the gradient and Laplacian of the area per lipid. This is consistent with what was previously derived in Deseri et al. (2008) from a dimension reduction procedure. The effective energy for the two-dimensional membrane turns out to depend upon the areal stretch and on the misalignment between the normal to the mid-surface and the orientation of the axes of the lipids. There, after enforcing the quasi-incompressibility of the membrane, it is shown that the bending splay modulus is determined by the phase of the lipids, i.e., the value of the thickness in the current configuration of the lipids through the derivative of the membrane part of the energy, and it is proved that the same modulus penalizes the gradient of the area changes. Recently in Deseri and Zurlo (2013), among other things, this approach allowed for obtaining the line tension detected across lipid rafts. Models of this type provide insight into how the thickness of the membrane can vary in response to protein insertions or antimicrobial peptides.

Lipid molecules, however, are generally not aligned normal to the membrane surface (Fig. 1). For example, the tilt angle of gel-phase DPPC was found to be approximately 32° (Tristram-Nagle et al. 1993). Even in the liquid phase, lipids can tilt in regions adjacent to protein inclusions (Watkins et al. 2011) (Fig. 1e, f). Membrane fission and fusion is a critical cellular process that takes place at lengths comparable to the lipid length. Membrane fusion has been studied using dissipative particle dynamics (DPD) approaches (Grafmuller et al. 2007, 2009). These studies have shown that when two fusing membranes are in close proximity, the lipids tilt, splay and flip from one monolayer to another (Grafmuller et al. 2007, 2009; Marrink and Mark 2003).

Lipid tilt as a key degree of freedom has been explored previously in continuum models (Lubensky and MacKintosh 1993; Kuzmin et al. 2005; Hamm and Kozlov 2000, 1998; May 2000). Most of these models are based on the assumption that the lipid tilt angle is small and bending is the dominant term in the membrane potential energy. An early theory of orientational order in chiral molecules was developed by Helfrich and Prost (1988), who showed that a chiral membrane in a tilted phase will form a cylinder because of the bending and packing introduced by lipid tilt variation. Similarly, Selinger et al. (1996) have developed a theory for cylindrical tubules and helical ribbons formed from chiral lipid membranes where tilt is the key order parameter. In this study, they showed that tubules undergo a first-order transition from a uniform state to a helically modulated state, with periodic stripes in the tilt direction and ripples in the curvature.

While these models have provided substantial insight into the role of lipid tilt in modulating helical structures and other long-range effects, several open questions remain. Most importantly, what happens when the tilt angles of the lipids are not small, and when the lipids are allowed to flip between adjacent monolayers, as observed in simulations of fusion and fission? How does the changing tilt of the lipids influence the curvature and surface properties of the membrane such as surface tension and stretching? How does insertion of a protein change lipid tilt in its neighborhood? To answer these questions, we have developed a continuum model for the lipid membrane with tilt as the key degree of freedom and where the tilt can be large. Using this framework, we are able to model the orientation of the lipids along with the shape of the surface. We use this model to study tilt angle variations in response to protein insertions in the membrane and compare the results with a coarse-grained (CG) model of the bilayer membrane.

The paper is organized as follows: In Sect. 2, we provide a general framework for a 2D director model. In Sect. 3, we develop a continuum model for lipid tilt in 1D and derive the Euler equations. We identify the invariants in the system and construct a free energy that allows for membrane stretch, lipid tilt and gradient in lipid tilt. In Sect. 4, we describe the development of the CG DPD model that is used to validate the continuum model. In Sect. 5, we describe a few special cases of the tilt model, including reduction in the Helfrich model and spontaneous tilt. In Sect. 6, we compare the CG and continuum models for the membrane response to protein insertion in the membrane. We discuss the model applications and elaborate on the results obtained from the CG and continuum models in Sect. 7.

2 General model for lipid tilt

We provide here a general model for biological membranes with lipid tilt as the key degree of freedom. We consider a deformation map $\chi(\mathbf{x})$ that carries the material point $\mathbf{x}$ in a reference configuration κ_r to a current configuration κ_c. A director field $\mathbf{D}$ is associated with each material point $\mathbf{x}$ on κ_r (Fig. 1a). The classical Frank energy for three-dimensional liquid crystals takes the form (Virga 1994)

$$U=\underbrace{\frac{1}{2}k_1(\mathrm{div}\mathbf{D})^2}_{\text{Splay}}+\underbrace{\frac{1}{2}k_2(\mathbf{D}\cdot\mathrm{curl}\mathbf{D})^2}_{\text{Twist}}+\underbrace{\frac{1}{2}k_3|(\mathrm{grad}\mathbf{D})\mathbf{D}|^2}_{\text{Bend}}, \quad (1)$$

where $k_{1–3}$ are the positive constants.

Lipids are widely considered to be liquid crystal systems. Thus, if one derives the free energy of a thin liquid crystal film from the bulk energy, then, as shown in Steigmann (2013), the relevant film energy depends only on (1) the surface normal **n**, (2) the director **d** and (3) the director gradient $\nabla\mathbf{d}$. Here, **d** is the restriction of **D** to the surface ω (Fig. 1a). Then, the energy density per unit area for a thin film of liquid crystals (in this case a lipid bilayer) is given by Steigmann (2013)

$$\overline{W}(\mathbf{n},\mathbf{d},\nabla\mathbf{d})=|\mathbf{n}\cdot\mathbf{d}|U(\mathbf{n},\mathbf{d},\nabla\mathbf{d}) \quad (2)$$

This choice of $\overline{W}$ determines the optimal value of energy density per unit area with respect to $\nabla\mathbf{d}$; the result is an energy that is quadratic in $\nabla\mathbf{d}$, whenever the dependence of U on grad**D** is quadratic. The total energy of the surface ω is then given by

$$E=\int_\omega \overline{W}(\mathbf{n},\mathbf{d},\nabla\mathbf{d})\mathrm{d}a \quad (3)$$

Therefore, the energy can depend only on **n**, **d** and $\nabla\mathbf{d}$.

In the next Section, we specialize this model to 1D membranes.

3 Continuum model for 1D lipid tilt

3.1 Notation and assumptions

We develop a 1D model of the membrane with lipid tilt as the key degree of freedom. The 1D nature of the model provides us with the simplest mathematical framework to study the effect of tilt on membrane curvature and connect the continuum description with DPD simulations.

We consider planar curves characterized by position **r**(*s*), normal **n**(*s*), the tangent $\boldsymbol{\tau}(s)$ and the director **d**(*s*), where *s* is the arc length along the membrane (Fig. 1b). The surface normal **n** is determined by $\boldsymbol{\tau}$ in the present model. This arc length is along the deformed configuration, and this can be mapped to a reference configuration *S*. The binormal, **b**(*s*), is constant. The director **d** can be written in terms of its components as

$$\mathbf{d}=\beta\boldsymbol{\tau}+\gamma\mathbf{n} \quad (4)$$

In the case of a monolayer, the length of the director is the length of the lipid; for a bilayer, it is the combined length of the two lipids that span the bilayer. In both cases, we shall assume that the length of the director d_0 is constant, i.e., $d_0^2=\beta^2+\gamma^2$, and therefore, the

thickness can be inferred from the tilt. This constraint is implemented using a Lagrange multiplier, α. We do not assume that the membrane is incompressible; so, we allow the membrane to stretch in response to the forces acting on it. The complete list of variables and parameters used in the model is given in Table 1.

W is the energy per unit length of the membrane. We denote position by $\mathbf{r}(S)$, the unit tangent by $\boldsymbol{\tau}$ and the director by $\mathbf{d}$, where S is the arc length in the reference configuration. The $()'$ notation indicates derivative with respect to S, $\dot{()}$ is the variational derivative, and subscripts denote derivatives with respect to the indicated variable.

The dilation λ is given by

$$\lambda = |\mathbf{r}'(S)| = \frac{\mathrm{d}s}{\mathrm{d}S} \quad (5)$$

The total elastic energy of the membrane is

$$E = \int_c W \mathrm{d}s = \int_C \lambda W \mathrm{d}S \quad (6)$$

Let $\lambda W = \Psi$. The variational derivative of the energy is then given by

$$\dot{E} = \int_C \dot{\Psi}\, \mathrm{d}S \quad (7)$$

The energy W can depend on the vectors $\boldsymbol{\tau}$, $\mathbf{d}(S)$ and $\mathbf{d}'(S)$ (see Sect. 2). The following scalars can be constructed from these vectors: $\mathbf{d}\cdot\mathbf{d}$, $\boldsymbol{\tau}\cdot\mathbf{d}$, $\boldsymbol{\tau}\cdot\mathbf{d}'$, $\mathbf{d}'\cdot\mathbf{d}'$, $\mathbf{d}\cdot\mathbf{d}'$ and $\boldsymbol{\tau}\times\mathbf{d}\cdot\mathbf{d}'$. These scalars are determined by the 3 variables $\mathbf{d}\cdot\mathbf{d} = d$, $\boldsymbol{\tau}\cdot\mathbf{d} = \beta$ and $\boldsymbol{\tau}\cdot\mathbf{d}' = \eta$, which therefore constitute the list upon which W can depend.

Then, using the chain rule on Ψ, we have

$$\dot{\Psi} = \Psi_d\, \dot{d} + \Psi_\beta\, \dot{\beta} + \Psi_\eta\, \dot{\eta} + \Psi_\lambda\, \dot{\lambda}, \quad (8)$$

where Ψ_β is the partial derivative of Ψ with respect to β and so on, and

$$\dot{d} = d^{-1}\mathbf{d}\cdot\dot{\mathbf{d}} \quad (9)$$

$$\dot{\beta} = \mathbf{u}'\cdot\mathbf{d} + \mathbf{r}'\cdot\dot{\mathbf{d}} \quad (10)$$

$$\dot{\eta} = \mathbf{u}'\cdot\mathbf{d}' + \mathbf{r}'\cdot\dot{\mathbf{d}}' \quad (11)$$

The variational derivative of the membrane dilation λ is

$$\dot{\lambda} = \tfrac{1}{2\lambda}(\dot{\lambda}^2) = \tfrac{1}{2\lambda} 2\mathbf{r}'(S) \cdot \dot{\mathbf{r}}'(S) \quad (12)$$

$$= \boldsymbol{\tau}(S) \cdot \mathbf{u}'(S), \quad (13)$$

where $\mathbf{u}'(S) = \dot{\mathbf{r}}'(S)$.

We impose $d = d_0$ = constant via a Lagrange multiplier, α. Thus,

$$E = \int_C \Phi \mathrm{d}S, \quad \text{where} \quad (14)$$

$$\Phi = \Psi + \alpha(d - d_0), \quad \text{yielding} \quad (15)$$

$$\dot{E} = \int_C \dot{\Phi}\, \mathrm{d}S = \int_C (\dot{\Psi} + \alpha\, \dot{d})\mathrm{d}S = \int_C [-(\Phi_{\mathbf{r}'})'] \cdot \dot{\mathbf{r}}\, \mathrm{d}S + \int_C [\Phi_{\mathbf{d}} - (\Phi_{\mathbf{d}'})'] \cdot \dot{\mathbf{d}}\, \mathrm{d}S \quad (16)$$

When there is a nonzero pressure difference across the membrane, the above equation becomes

$$\dot{E}^* = \int_C (\dot{\Psi} + \alpha\, \dot{d})\mathrm{d}S + P \int_C \lambda \mathbf{n} \cdot \dot{\mathbf{r}}\, \mathrm{d}S = \int_C [-(\Phi_{\mathbf{r}'})' + \lambda P \mathbf{n}] \cdot \dot{\mathbf{r}}\, \mathrm{d}S + \int_C [\Phi_{\mathbf{d}} - (\Phi_{\mathbf{d}'})'] \cdot \dot{\mathbf{d}}\, \mathrm{d}S \quad (17)$$

where $\dot{E}^*$ = *Edot; +* $\dot{W}$, and P is the pressure difference acting across the membrane. $\dot{W}$ accounts for the work performed by P against the normal component of the variation $\mathbf{n} \cdot \dot{\mathbf{r}}$. At equilibrium, $\dot{E}^*$ vanishes. The resulting Euler equations are

$$\underbrace{(\Phi_{\mathbf{r}'})'}_{\substack{\text{Force} \\ \text{per unit length}}} - \underbrace{\lambda P \mathbf{n}}_{\substack{\text{Pressure difference} \\ \text{across the membrane}}} = \mathbf{0} \quad (18)$$

$$\underbrace{(\Phi_{\mathbf{d}'})'}_{\substack{\text{Gradient} \\ \text{of bending moment}}} - \underbrace{(\Phi_{\mathbf{d}})}_{\substack{\text{Force associated with} \\ \text{changing the director} \\ \text{configuration}}} = \mathbf{0} \quad (19)$$

where

$$\Phi_{\mathbf{r}'} = \Psi_\beta \mathbf{d} + \Psi_\eta \mathbf{d}' + (\Psi + \Psi_\lambda)\boldsymbol{\tau} \quad (20)$$

$$\Phi_{\mathbf{d}} = d_0^{-1}(\Psi_d + \alpha)\mathbf{d} + \Psi_\beta \boldsymbol{\tau} \quad (21)$$

$$\Phi_{\mathbf{d}'} = \Psi_\eta \boldsymbol{\tau} \quad (22)$$

If the curve is not closed, the force acting on the membrane is given by $\Phi_{\mathbf{r}'}$ and the line tension along the membrane is given by the tangential component of this force: $(\Phi_{\mathbf{r}'}) \cdot \boldsymbol{\tau}$. The quantity $\Phi_{\mathbf{d}'}$ is analogous to a torque. The quantity $\Phi_{\mathbf{d}}$ is the force associated with changing the director configuration. In general, the boundary conditions for the differential equations in Eqs. (18) and (19) can be written for the position and director vectors or for the forces acting on the membrane boundaries.

3.2 Elastic energy of the membrane

As a special case of the foregoing formulation, we assume that the membrane elastic energy has the general form

$$\Psi = \underbrace{k_\lambda(\lambda-1)^2}_{\substack{\text{energy density associated} \\ \text{with stretch}}} + \underbrace{k_\eta \eta^2}_{\substack{\text{energy density associated} \\ \text{with tilt gradient} \\ \text{and curvature changes}}} + \underbrace{k_\beta(\beta-\beta_0)^2}_{\substack{\text{energy density associated} \\ \text{with tilt deviation from} \\ \text{the resting tilt angle } \beta_0}} \quad (23)$$

Note that the energy is quadratic in η, thereby satisfying the foregoing condition that the areal energy density be quadratic in the gradient of the director (see Sect. 2 and Steigmann 2013). Using this expression for the elastic energy in the Euler equations (Eqs. 18 and 19), with $P = 0$, results in the following ordinary differential equations for the shape of the membrane:

$$\begin{gathered} \frac{\Psi_\eta \beta H}{\gamma} + \Psi_\beta = \Psi_\eta' \\ \Psi_\beta' \beta + (\Psi_\beta + \Psi_\eta')' \eta + \Psi_\eta \left(\eta' + \frac{\eta \beta H}{\gamma}\right) + (\Psi + \Psi_\lambda)' = 0 \\ \Psi_\beta' \gamma + (\Psi_\beta + \Psi_\eta') \left(\frac{-\eta\beta}{\gamma}\right) \\ -\Psi_\eta \left(\frac{\eta^2 d_0^2}{\gamma^3} + \frac{\eta \beta^2 H}{\gamma^2} + \frac{\eta' \beta}{\gamma}\right) + H(\Psi + \Psi_\lambda) = 0 \\ \beta' = \eta + H\gamma \\ \gamma' = -\frac{\beta' \beta}{\gamma} \end{gathered} \quad (24)$$

The position $\mathbf{r}(S)$ can be written as

$$\mathbf{r}(S) = x(S)\mathbf{e_1} + y(S)\mathbf{e_2}, \quad (25)$$

where $\mathbf{e_1}$ and $\mathbf{e_2}$ are orthonormal basis vectors. Then, we can write

$$\mathbf{r}'(S) = x'(S)\mathbf{e_1} + y'(S)\mathbf{e_2}, \quad (26)$$

and the unit tangent and normal as

$$\boldsymbol{\tau} = \frac{x'(S)\mathbf{e_1} + y'(S)\mathbf{e_2}}{\sqrt{x'^2 + y'^2}} \qquad \mathbf{n} = \frac{y'(S)\mathbf{e_1} - x'(S)\mathbf{e_2}}{\sqrt{x'^2 + y'^2}} \quad (27)$$

From Eqs. (5 and 26), we find $\lambda = \sqrt{x'^2 + y'^2}$. We use the arc length parametrization to obtain the additional equations

$$x' = \lambda\cos(\theta) \quad y' = \lambda\sin(\theta) \quad \text{and} \quad \theta' = -2H\lambda. \quad (28)$$

Together, Eqs. 24 and 28 describe the system. Boundary conditions will depend on the specific situation.

To test the predictive potential of the continuum model, we compare the tilt angle distributions when proteins are inserted in the membrane using a previously developed CG DPD model (Kranenburg et al. 2003; de Meyer et al. 2008; Benjamini and Smit 2012).

3.3 Parameters

The main parameters in the model are the moduli corresponding to the invariants η and β. We use a value of $17k_BT$ for the membrane bending modulus obtained from the CG model discussed below. The bilayer thickness and k_η were also estimated from the CG model. All parameters are listed in Table 2. To ensure consistent units in the 1D model, we assume that the width of the membrane is 1 length unit.

4 Description of the coarse-grained model

In this work, we used the CG model previously published by Benjamini and Smit (2012). Three system components were modeled: water, lipids and α-helices, using four distinct bead types. Each bead represents a set of three heavy atoms, on average, that are bundled together. The types of beads considered include the following: (1) a water like bead, *w*, used to describe a set of three water molecules; (2) a hydrophilic bead, *h*, used to model the lipid head group as well as the marginal part of the helix; (3) a hydrophobic tail bead, *t*, used to model the hydrophobic lipid tail; and (4) a hydrophobic protein bead, *p*, used to model the hydrophobic core of a transmembrane(TM) helix.

The lipid model was previously shown to form a stable bilayer structure and to reproduce the typical phase behavior of lipid bilayers (Kranenburg et al. 2003). It includes a head group consisting of three *h* types of beads and two tails each containing five *t* types of beads (see Fig. 2a).

The helix model captures the basic common characteristic of all TM helices. It contains a helical geometry of beads with a hydrophobic core and hydrophilic caps on both ends. Such

a model guarantees that the helix will remain within the membrane, while both its ends are exposed to the hydrophilic phase on the bilayer (or water). For more details on model parameters, see Benjamini and Smit (2013).

4.1 Simulation technique

We studied the CG model system using a hybrid dissipative particle dynamics-Monte Carlo (DPD-MC) simulation technique. In DPD, a set of three forces combine together: a conservative force, $\mathbf{F}^C$, a dissipative force $\mathbf{F}^D$ and a random force $\mathbf{F}^R$ (Groot and Warren 1997). The conservative force includes all bonded and non-bonded interactions. The non-bonded interactives involve a soft core repulsive force whose amplitude is based on the types of the two interacting beads. Repulsive interaction parameters for our modeled beads are shown in Table 3. Each interaction parameter represents the maximal repulsion between beads of each type in reduced units of $[\varepsilon_0/l_0]$. For example, the repulsion between a hydrophobic bead and water (a_{wt} = 80.0) is set higher than that of a hydrophilic bead and water (a_{wh} = 15.0). The non-bonded contribution to the conservative force, $\mathbf{F}^C$, depends on these interaction parameters, such that: $\mathbf{F}_{ij}^C(\mathbf{r_{ij}})=a_{ij}(1-r_{ij}/\mathscr{R})\cdot\hat{r}_{ij}$ for $r_{ij} < \mathcal{R}$; and 0.0 otherwise. The dissipative and random forces mimic the friction and random collisions between close molecules, respectively. When balancing the random and dissipative forces to satisfy the fluctuation-dissipation theorem, the overall effect is a system simulated at constant temperature with equilibrium system configurations determined solely by the conservative (bonded and non-bonded) forces. All forces are applied on a pairwise basis in the direction of the vector connecting the beads. DPD forces are truncated at a predefined cutoff radius ($\mathcal{R} = 1l_0 \sim 6.46$ Å; l_0 is a reduced length unit) and satisfy $\mathbf{F}_{ij} = -\mathbf{F}_{ji}$ such that the total momentum of the system is conserved. The positions and velocities were integrated using the modified Velocity–Verlet algorithm (Groot and Warren 1997).

We used Monte Carlo moves to sample from the $NP_\perp\gamma T$ ensemble. The bilayer surface tension, γ, was set to zero to simulate the tensionless state of unconstrained lipid bilayers (Jahnig 1996; Marrink et al. 2001). The normal pressure, $P_\perp$, was set equal to the bulk water pressure. To combine the DPD and MC technique and maintain detailed balance, each simulation step, we chose at random between a short DPD trajectory, a constant surface tension move or a constant normal pressure move. Note that in all MC moves, the overall volume of the system is kept constant. For a detailed description of the simulation technique and parameters, we refer to previously published work (de Meyer et al. 2010).

4.2 Sampling methods

In the course of our CG simulation, we sampled the tilt of lipids in the vicinity of TM helices. The lipid tilt angle is defined by the position of lipid tails, as shown in Fig. 2b. We defined a vector connecting the center-of-mass of the first two tail beads (first out of five beads in each tail) to the center-of-mass of the two last tail beads (fifth out of five beads in each tail). The lipid tilt is then defined as the angle between the constructed vector and the $+\hat{z}$ direction.

To obtain the tilt angle of lipids around one inserted TM helix, we sampled lipids as a function of their radial distance from the helix (see Fig. 2c, d). In each time frame, we

looped over several radii away from the helix center-of-mass ($r_i = \{1, 2, \ldots, 10\}$ l_0). For each radii bin, i, we maintained all lipids within the range $r \in [r_i - 1.0, r_i)$ of the helix center-of-mass. As the number of lipids in each bin grows with the radius, we randomly chose a subset of the lipids in each bin, such that all bins will contain approximately the same number of samples. To that end, we chose to sample a lipid with probability $P(r_i) = 1/(2r_i - 1)$. Note that all the lipids in the bin $r_i = 1.0$ l_0 are sampled, and all consecutive bins will contain a similar number of lipids.

5 Special cases of the tilt model

5.1 Reduction in Helfrich model

The model for elastic membranes developed by Helfrich assumes that only curvature elasticity is important for determining the shapes of closed vesicles. However, Helfrich notes at the very outset that lipid tilt and membrane stretch can be important variables. In developing his model, Helfrich assumes that the lipids are always aligned normal to the bilayer (Helfrich 1973). To recover the Helfrich model from the tilt model, we have to impose three additional constraints (Fig. 3a):

$$\frac{\mathbf{d}}{d_0}=\mathbf{n}, \quad \frac{\mathbf{d}'}{d_0}=\mathbf{n}'=-H\boldsymbol{\tau} \quad \text{and} \quad \lambda=1 \quad (29)$$

Eq. $29_{(1)}$ states that the director is aligned normal to the membrane everywhere. Since the director and director gradient are independent at a given point, we have to specify how the director gradient varies. Equation $29_{(2)}$ states that the director gradient must vary like the gradient of the normal to the surface (Fig. 3a). Since the gradient of the normal is the mean curvature, the director gradient captures the variation of curvature along the surface. The constraint on λ holds the membrane stretch to unity. The constraints in Eq. 29 can be written as

$$\lambda=1, \quad \beta=0 \quad \text{and} \quad \eta=-Hd_0 \quad (30)$$

everywhere on the membrane. These are in addition to the constraint $d = d_0$. Therefore, we need additional Lagrange multipliers to impose these constraints. The auxiliary energy potential now becomes

$$\zeta=\lambda W+\mu(\lambda-1)+\alpha(d-d_0)+m_1(\beta-0)+m_2(\eta+Hd_0), \quad (31)$$

where μ, m_1 and m_2 are Lagrange multipliers for the constraints presented in Eq. 29, respectively.

$$\dot{\zeta} = \dot{\lambda}\,(W+\mu)+\lambda\,\dot{W}+\overline{\mu}\,\dot{d}+m_1\,\dot{\beta}+m_2\,\dot{\eta} \quad (32)$$

We use Eq. 9 to obtain

$$\begin{aligned}\zeta_{\mathbf{r}'} &= (W_\beta + m_1)\mathbf{d} + (W_\eta + m_2)\mathbf{d}' + (W + \mu)\boldsymbol{\tau} \\ \zeta_{\mathbf{d}} &= d_0^{-1}(W_d + \bar{\mu})\mathbf{d} + (W_\beta + m_1)\boldsymbol{\tau} \\ \zeta_{\mathbf{d}'} &= (W_\eta + m_2)\boldsymbol{\tau},\end{aligned} \quad (33)$$

and the Euler equations become

$$(\zeta_{\mathbf{r}'})' = -P\mathbf{n} \quad (34)$$

$$(\zeta_{\mathbf{d}'})' - \zeta_{\mathbf{d}} = \mathbf{0} \quad (35)$$

Expanding out these equations will yield equations involving the second derivative of curvature and result in the well-known ‘shape equation’ (Steigmann 1999). The energy is now $W = k_\eta \eta^2 = k_\eta d_0^2 H^2$, and the moduli k_η and k_b can be related by $k_b = k_\eta d_0^2$.

In the simple case that H is constant everywhere, simulations yield a circle for positive pressure difference P and a straight line for $P = 0$. Figure 3b, c shows schematics of the Helfrich case of lipid membranes. We do not include further simulations from the Helfrich model, since these have been studied extensively elsewhere (Seifert et al. 1991; Jaric et al. 1995).

5.2 Spontaneous tilt

The simplest case of the continuum model is where all the lipids are aligned along the same nonzero tilt, with zero tilt gradient. By writing the energy as $W = k_\beta(\beta - \beta_0)^2 + k_\lambda(\lambda - 1)^2$, we establish the general case where the resting tilt angle is β_0. This energy is minimized when $\beta = \beta_0$. Since there are no a priori assumptions on the tilt angle, β_0 need not be 0. Just as the spontaneous curvature of the lipid captures, the curvature of the membrane that minimizes the bending energy, the resting tilt, β_0, represents the intrinsic tilt along which the lipids align themselves. It can be thought of as the spontaneous tilt of the lipids.

In this case, the ODEs reduce to a set of algebraic equations given by

$$\begin{aligned}\beta &= \beta_0 \\ \Psi + \Psi_\lambda &= \text{constant} \\ H &= \frac{-P}{\Psi + \Psi_\lambda}\end{aligned} \quad (36)$$

Thus, the equation for mean curvature is similar to the capillarity equation $H = -P/\sigma$. In Fig. 3d, we show a depiction of lipids aligned at a resting angle away from the normal, when $P = 0$. When P is not zero, the curvature is computed by Eq. $36_{(3)}$ and is shown in Fig. 3e. In this case, the line tension is given by $\sigma = \Psi + \Psi_\lambda$.

6 Lipid tilt due to helix insertion

We consider the situation where a helix is inserted into the membrane and causes the lipids in the neighboring region to tilt. In the continuum model when one protein helix is

introduced into the membrane, the mathematical problem reduced to solving a boundary value problem on a semi-infinite domain. At the point of helix insertion ($s = 0$), the tilt angle introduced by the helix is known; i.e., β and γ are known at this boundary. Each helix introduces a different tilt angle at $s = 0$ (Fig. 4). Additionally, we can specify the position of the membrane at $s = 0$ as $x = 0$ and $y = 0$. Far away from the helix insertion, the membrane has bulk values of lipid tilt and line tension. We solve the ODEs given in Eq. 24 using the energy given in Eq. 23 along with the specified boundary conditions. The CG model provides the value of lipid tilt far away from the protein helix as $\beta_0 = d_0\cos(24°)$ and $(\Phi_{\mathbf{r}'}) \cdot \boldsymbol{\tau} = 0$. These boundary value problems were solved using the math interface of COMSOL Multiphysics ® using a domain length of 15 nm.

6.1 Comparison with the coarse-grained model

The continuum model is suitable for investigating membrane phenomena at a mesoscopic scale, that is, on the scale of the membrane thickness. Here, we show that the continuum model captures behavior corresponding to processes operating at the molecular scale by comparing its predictions with a CG model subjected to DPD. In the CG model, lipids, membrane-embedded proteins and water are represented by strings of beads (Fig. 2a, b).

In order to draw direct comparisons between the CG and the continuum models, we observe that the CG simulations were performed on a torus with periodic boundary conditions. If the torus is large enough, then locally it is nearly cylindrical, whereas our 1D theory provides a model with cylindrical cross-sections. We show below that the 1D model yields a surprisingly good approximation to the CG simulations in this setting.

6.2 Lipid tilt induced by one protein

In these simulations, we explored helices of various sizes. We varied the number of helix residues, such that all helices have the same number of hydrophilic residues on both ends (three), but a different number of hydrophobic residues at their center. Helices 1–4 correspondingly contain 9, 12, 15 and 18 hydrophobic residues at their center, respectively. Varying the number of hydrophobic residues allowed us to control the hydrophobic mismatch between the helices and the bilayer. Here, we focus only on negative (helix 1–3, $\Delta d = 13.27, 8.77, 4.27$ Å, respectively) and zero (Helix 4, $\Delta d = 0.23$ Å) hydrophobic mismatches, which share similar bilayer response characteristic to their inclusion, but vary in their degree. The tilt angle induced by each helix is shown in Fig. 4.

The CG simulations predict that the lipids attain the bulk tilt value within 4–6 nm from the helix insertion (Fig. 5a, b). Using values of $k_\beta = 40$ pN/nm^2 from the literature (Hamm and Kozlov 2000; May et al. 2004) did not give us good matches for the tilt angle distribution along the arc length as observed in the CG simulations (Fig. 9). However, when the value of k_β was set to be less than k_{η}, at 1 pN/nm^2, we were able to obtain good agreement for the tilt angle distribution between the continuum and CG models for all four helices (Fig. 5). The inset in each panel of (Fig. 5) shows a snapshot of the membrane with the helix inserted. The alignment of the helix changes from Helix 1 to Helix 4 as seen in these snapshots. The alignment of Helix 4 is closest to the bulk bilayer value of 24° (Fig. 5d). In all four cases, the lipid tilt attains the bulk value within 4–6 nm.

In our model, we were able to obtain k_η from k_b measurements from the CG model and the stretch modulus of a bilayer is widely documented as being quite high (Lipowsky and Sackmann 1995). The unknown parameter is the tilt modulus k_β. Previous estimates of the tilt modulus state that it can range from 0.002 k_BT/nm^2 (May et al. 2004) to 40 pN/nm (Hamm and Kozlov 2000). We ran simulations with different values of the tilt modulus (Fig. 9) and found the best match between the continuum and CG model when $k_\beta = 1$ pN/nm. Increasing k_β decreases the distance over which the tilt angle goes to its resting angle (Fig. 9) and is not in agreement with the observations in the CG model.

6.3 Membrane thickness

Insertion of a protein helix will cause a local tilt gradient around the protein. This in turn creates membrane thinning around the protein. In the continuum model, membrane thickness is given by γ. That is, as the tilt angle induced by the protein increases, membrane thickness decreases in the region around the protein. Helix 1 causes the most thinning and Helix 4 causes the least thinning (Fig. 6a).

We measured the thickness of the bilayer in the CG model as a function of distance from the helix center-of-mass by extracting the positions of lipid heads (second bead out of three head beads) in a total of 1,600 time frames. We calculated the distance between each lipid and the helix center-of-mass and obtained a detailed map of the upper and lower layer head bead positions at each time frame. To gain better statistics, we bundled together every 100 frames. For each group of frames, we extrapolated the height of the lower and upper bilayer leaflets on a radial grid using the LOESS method (Chambers and Hastie 1992). The average bilayer thickness as a function of distance from helix center is then inferred by subtracting the grids of the upper and lower leaflets.

In the CG simulations, the bilayer changes its properties to fit the helix. As a result, the helices that induce larger tilt angle changes also result in greater changes in membrane thickness (Fig. 6b). The thickness variation relaxes at the same length scale of 4–6 nm as the tilt angle. Not surprisingly, the trend of membrane thinning in response to protein-induced lipid tilt was the same in both models, but the exact values of the membrane thickness did not match.

6.4 Membrane stretch and line tension

In addition to changing lipid tilt angle and thickness, the continuum model also allows the membrane a small degree of stretch, between 1 and 1.2 % in the 4–6 nm distance from the helix (Fig. 7a). The extent of stretch decreases as the tilt angle decreases. This is consistent with the idea that larger deviations from the bulk tilt angle will cause larger strain on the membrane. Lipid membranes are more resistant to dilation than to bending (Secomb and Skalak 1982; Evans and Skalak 1980) and even modest values of stretch can cause membrane rupture (Rawicz et al. 2008).

Additionally, the line tension $((\Phi_{\mathbf{r}'}) \cdot \boldsymbol{\tau})$ is highest for the largest tilt angle difference (Fig. 7b) and decreases with decreasing tilt angle. Far away from the helix insertion, the line tension goes to zero.

6.5 Energy contributions

The relative contributions of the tilt energy, η energy and the stretch energy are shown in Fig. 8. In all cases, the energy contribution from membrane stretch is the smallest of the three terms. For the helix that induces the largest tilt angle difference, the maximum energy penalty is from the tilt term. The energy density that captures curvature changes $k_\eta \eta^2$ is smaller than the tilt energy $k_\beta(\beta - \beta_0)^2$. For small tilt angle differences between the helix insertion and the bulk bilayer, the stretch energy is negligible, consistent with the observations of very small stretch (Fig. 7). As the difference in tilt angles decreases, the ratio of tilt energy to η energy decreases. The variation of energy with the modulus, k_β, is shown in Fig. 9. Increasing the tilt modulus will increase the tilt energy contribution. In all variations, we found that the energy contribution from tilt is higher than the energy contribution from the curvature coupled term η. Therefore, in regions close to a protein insertion, the largest energy contribution comes from lipid tilt, followed by η and then by lipid stretch.

7 Conclusions

Lipid tilt is a key degree of freedom in lipid membranes. Membrane lipids change their orientation to relieve the stresses that are induced by protein inclusions and by processes such as membrane fusion and fission. Additionally, the membrane is the first point of contact for many viruses. Viral fusion proteins from the influenza virus, HIV and Ebola virus can all insert into the membrane and drive a local rearrangement of the lipids so as to create a fusion pore (Phillips et al. 2009; Nir and Nieva 2000; Fischer and Hsu 2011). Antimicrobial peptides such as bacterial gramicidin work by inserting the gramicidin helix into the membrane; this changes the lipid orientation to form a channel in the bilayer (Lundbaek et al. 2010). The influence of proteins on lipids is not unidirectional; many proteins modulate their activity in response to the lipids that bind to them, or to the bilayer thickness and/or lipid curvature. All of these processes involve local rearrangements of the lipid orientation and thus the membrane curvature. In order to understand these phenomena, it is important to capture the smallest length scale on which these spatial rearrangements take place. The orientation of lipids is the obvious length scale on which to capture these changes.

Hamm and Kozlov have derived a model for the lipid bilayer that includes lipid tilt and splay using the Frank liquid crystal energies (Hamm and Kozlov 2000, 1998). Their definition of the tilt vector differs from our use of the director; however, these models complement each other because the tilt gradient and mean curvature are coupled in both. The Hamm and Kozlov model has been used to study line tension (Kuzmin et al. 2005), protein inclusion (Kozlovsky et al. 2004) and hemifusion intermediates (Kozlovsky et al. 2002; Kozlovsky and Kozlov 2002). While many studies have noted that lipid tilt could be important in accommodating protein inclusions in the membrane, experimental measurements of lipid orientation in the fluid phase have not yet been obtained. Kozlovsky et al. predicted that, at small tilt angles and in the presence of a protein inclusion, membrane bending is more important than lipid tilting (Kozlovsky et al. 2004). Moreover, in the regime of small tilt angles, lipid flipping, an important step in scission, is not possible.

We have presented here a one-dimensional model of lipid membranes, readily generalizable to higher dimensions (Steigmann 2013), using tilt as the fundamental degree of freedom. Importantly, we do not impose any restrictions on the range of the tilt angle. We emphasize that our 1D model limits the kind of shapes we can generate and in obtaining certain finer length scale effects. While we are able to obtain good agreement between the 1D model and the averaged behavior from the CG model, a full surface model is required for capturing further details of membrane deformations. Additionally, we are using one director to capture two-tailed lipids. To represent the two tails, the director model may be extended to include two directors, one for each tail. Our current efforts are focusing on developing this in a higher dimensional framework.

In the 1D case, the elastic equilibria are the solutions of a system of ODEs that govern the variation of tilt, curvature and stretch along the arc length. These equations can be solved simultaneously with the appropriate boundary conditions to obtain the membrane shape and tilt distribution for various scenarios. We apply this tilt model to the case where a protein is inserted into the lipid bilayer and compare the results computed from the continuum model to the results from a coarse-grained molecular dynamics model for the same scenario. This model reduces to the Helfrich model when the lipids are all aligned normal to the surface and where the curvatures are small (Helfrich 1973) (See Fig. 3a–c). When the membrane is composed of a single lipid species with constant tilt, the result is similar to membranes where DPPC packs in a gel-phase bilayer aligned at 32° (Tristram-Nagle et al. 1993) (See Fig. 3d, e).

We compared the continuum model with a CG molecular model of lipid bilayers with protein inclusions. This comparative framework is the closest we can get to an experimental measurement at this time. We find that a single protein helix introduces a tilt gradient that extends 5–6 nm from the helix (Fig. 5).

Hydrophobic mismatch is the difference between the hydrophobic size of the helix and that of the membrane. Whenever such mismatch arises, the lipids and helix reorganize so as to minimize the exposure of hydrophobic beads to water or other hydrophilic beads (Benjamini and Smit 2013; Killian et al. 1996; Park and Opella 2005; Lee and Im 2008; Parton et al. 2011; Strandberg et al. 2012). In negatively mismatched helices, most of the adjustments are found in the lipids surrounding the helix, rather than in the helix itself. This is because the helix's principal degree of freedom is its tilt, which does not help minimize the exposure of hydrophilic beads (Benjamini and Smit 2013). In our simulations, we observe that hydrophobic mismatch affects both the lipids' tilt (Fig. 5) and the membrane thickness close to the helix center (Fig. 6). The membrane thickness surrounding the helix decreases and the membrane shrinks to accommodate the presence of the helix. The thickness drop corresponds to the helix hydrophobic mismatch (Fig. 6). Additionally, the lipids surrounding a helix tilt to a greater extent when surrounding a very negatively mismatched helix (Fig. 4), in order to shield the lipid tails from the water. We are able to obtain the same tilt characteristics in the continuum model, by allowing the tilt modulus $k_\beta \approx 1$ pN/nm^2. Using the CG and continuum models in tandem, we predict that lipid tilt angle changes are an important contribution at short length scales.

Based on the above observations, we propose that membrane curvatures that occur on length scales of the bilayer thickness are dominated by lipid tilt. Ignoring the tilt energy contributions by assuming that the tilt angle is small will miss the change in tilt angle in small regions. The CG model shows that the lipids are fluctuating and the bulk tilt angle is approximately 24°. These effects may not be relevant while studying large curvatures such as vesicle shapes; however, these effects can dominate when multiple proteins aggregate or during membrane fusion and fission. Our future studies will focus on these phenomena.

Acknowledgments

The authors would like to thank Dr. Kranthi Kiran Mandadapu and Shachi Katira for many stimulating discussions. This work was funded in part by NIH 1R01GM104979-01 awarded to G.O. A.B. was supported by the Director, Office of Science, Office of Basic Energy Sciences, Division of Chemical, Geological and Biosciences of the U.S. Department of Energy under Contract No. DE-AC02-05CH11231.

References

Benjamini A, Smit B. Robust driving forces for transmembrane helix packing. Biophys J. 2012; 103:1227–1235. [PubMed: 22995495]

Benjamini A, Smit B. Lipid mediated packing of transmembrane helices—a dissipative particle dynamics study. Soft Matter. 201310.1039/C2SM27165F

Bitbol A-F, Constantin D, Fournier J-B. Bilayer elasticity at the nanoscale: the need for new terms. PLoS One. 2012; 7(11):e48306. [PubMed: 23144862]

Bloom M, Mouritsen OG. Mattress model of lipid-protein interactions in membranes. Biophys J. 1984; 46(2):141. [PubMed: 6478029]

Chambers, JM.; Hastie, T. Statistical models in S. Wadsworth & Brooks/Cole computer science series. Wadsworth & Brooks/Cole Advanced Books & Software; Pacific Grove, Calif: 1992.

de Meyer FJM, Venturoli M, Smit B. Molecular simulations of lipid-mediated protein-protein interactions. Biophys J. 2008; 95(4):1851–1865. [PubMed: 18487292]

de Meyer FJM, Benjamini A, Rodgers JM, Misteli Y, Smit B. Molecular simulation of the DMPC-cholesterol phase diagram. J Phys Chem B. 2010; 114(32):10451–10461. [PubMed: 20662483]

Derényi I, Jülicher F, Prost J. Formation and interaction of membrane tubes. Phys Rev Lett. 2002; 88(23):238101. [PubMed: 12059401]

Deseri L, Piccioni MD, Zurlo G. Derivation of a new free energy for biological membranes. Cont Mech Thermodyn. 2008; 20(5):255–273.

Deseri L, Zurlo G. The stretching elasticity of biomembranes determines their line tension and bending rigidity. Biomech Model Mech Biol. 201310.1007/s10237-013-0478-z

Deuling HJ, Helfrich W. Red blood cell shapes as explained on the basis of curvature elasticity. Biophys J. 1976; 16(8):861–868. [PubMed: 938726]

Evans, EA.; Skalak, R. Mechanics and thermodynamics of biomembranes. CRC Press; Boca Raton: 1980. Mechanics and thermodynamics of bio-membranes.

Fischer WB, Hsu H. Viral channel forming proteins-modeling the target. Biochimica et biophysica acta. 2011; 1808(2):561–571. [PubMed: 20546700]

Grafmuller A, Shillcock J, Lipowsky R. Pathway of membrane fusion with two tension-dependent energy barriers. Phys Rev Lett. 2007; 98(21):218101. [PubMed: 17677811]

Grafmuller A, Shillcock J, Lipowsky R. The fusion of membranes and vesicles: pathway and energy barriers from dissipative particle dynamics. Biophys J. 2009; 96(7):2658–2675. [PubMed: 19348749]

Groot RD, Warren PB. Dissipative particle dynamics: bridging the gap between atomistic and mesoscopic simulation. J Chem Phys. 1997; 107(11):4423–4435.

Hamm M, Kozlov MM. Tilt model of inverted amphiphilic mesophases. Eur Phys J B. 1998; 6(4): 519–528.

Hamm M, Kozlov MM. Elastic energy of tilt and bending of fluid membranes. Eur Phys J E. 2000; 3:323–335.

Helfrich W. Elastic properties of lipid bilayers: theory and possible experiments. Z Naturforsch. 1973; 28(11):693–703.

Helfrich W, Prost J. Intrinsic bending force in anisotropic membranes made of chiral molecules. Phys Rev A. 1988; 38(6):3065–3068. [PubMed: 9900723]

Iglic A. A possible mechanism determining the stability of spiculated red blood cells. J Biomech. 1997; 30(1):35–40. [PubMed: 8970922]

Jahnig F. What is the surface tension of a lipid bilayer membrane? Biophys J. 1996; 71(3):1348–1349. [PubMed: 8874009]

Jaric M, Seifert U, Wintz W, Wortis M. Vesicular instabilities: The prolate-to-oblate transition and other shape instabilities of fluid bilayer membranes. Phys Rev E Stat Phys Plasmas Fluids Relat Inter-discip Top. 1995; 52(6):6623–6634.

Killian JA, Salemink I, de Planque MRR, Lindblom G, Koeppe RE, Greathouse DV. Induction of nonbilayer structures in diacylphosphatidylcholine model membranes by transmembrane alpha-helical peptides: importance of hydrophobic mismatch and proposed role of tryptophans. Biochemistry. 1996; 35(3):1037–1045. [PubMed: 8547239]

Kozlovsky Y, Chernomordik LV, Kozlov MM. Lipid intermediates in membrane fusion: formation, structure, and decay of hemi-fusion diaphragm. Biophys J. 2002; 83(5):2634–2651. [PubMed: 12414697]

Kozlovsky Y, Kozlov MM. Stalk model of membrane fusion: solution of energy crisis. Biophys J. 2002; 82(2):882–895. [PubMed: 11806930]

Kozlovsky Y, Zimmerberg J, Kozlov MM. Orientation and interaction of oblique cylindrical inclusions embedded in a lipid monolayer: a theoretical model for viral fusion peptides. Biophys J. 2004; 87(2):999–1012. [PubMed: 15298906]

Kranenburg M, Venturoli M, Smit B. Phase behavior and induced interdigitation in bilayers studied with dissipative particle dynamics. J Phys Chem B. 2003; 107(41):11491–11501.

Kuzmin PI, Akimov SA, Chizmadzhev YA, Zimmerberg J, Cohen FS. Line tension and interaction energies of membrane rafts calculated from lipid splay and tilt. Biophys J. 2005; 88(2):1120–1133. [PubMed: 15542550]

Lee J, Im W. Role of hydrogen bonding and helix-lipid interactions in transmembrane helix association. J Am Chem Soc. 2008; 130(20):6456–6462. [PubMed: 18422318]

Lim GHW, Wortis M, Mukhopadhyay R. Stomatocytediscocyteechinocyte sequence of the human red blood cell: evidence for the bilayer couple hypothesis from membrane mechanics. Proc Natl Acad Sci. 2002; 99(26):16766. [PubMed: 12471152]

Lipowsky, R.; Sackmann, E. Structure and dynamics of membranes. 1. Elsevier; Amsterdam: 1995.

Lubensky TC, MacKintosh FC. Theory of “ripple” phases of lipid bilayers. Phys Rev Lett. 1993; 71(10):1565–1568. [PubMed: 10054440]

Lundbaek JA, Collingwood SA, Ingólfsson HI, Kapoor R, Andersen OS. Lipid bilayer regulation of membrane protein function: gramicidin channels as molecular force probes. J R Soc Interface R Soc. 2010; 7(44):373–395.

Marrink Siewert J, Mark Alan E. The mechanism of vesicle fusion as revealed by molecular dynamics simulations. J Am Chem Soc. 2003; 125(37):11144–11145. [PubMed: 16220905]

Marrink SJ, Lindahl E, Edholm O, Mark AE. Simulation of the spontaneous aggregation of phospholipids into bilayers. J Am Chem Soc. 2001; 123(35):8638–8639. [PubMed: 11525689]

May S. Protein-induced bilayer deformations: the lipid tilt degree of freedom. Euro Biophys J EBJ. 2000; 29(1):17–28.

May S, Kozlovsky Y, Ben-Shaul A, Kozlov MM. Tilt modulus of a lipid monolayer. Euro Phys J E Soft Matter. 2004; 14(3):299–308.

Nelson P, Powers T, Seifert U. Dynamical theory of the pearling instability in cylindrical vesicles. Phys Rev Lett. 1995; 17:3384–3387. [PubMed: 10058187]

Nir S, Nieva JL. Interactions of peptides with liposomes: pore formation and fusion. Prog Lipid Res. 2000; 39(2):181–206. [PubMed: 10775764]

Park SH, Opella SJ. Tilt angle of a trans-membrane helix is determined by hydrophobic mismatch. J Mol Biol. 2005; 350(2):310–318. [PubMed: 15936031]

Parton Daniel L, Klingelhoefer Jochen W, Sansom Mark SP. Aggregation of model membrane proteins, modulated by hydrophobic mismatch, membrane curvature, and protein class. Biophys J. 2011; 101(3):691–699. [PubMed: 21806937]

Phillips R, Ursell T, Wiggins P, Sens P. Emerging roles for lipids in shaping membrane-protein function. Nature. 2009; 459(7245):379–385. [PubMed: 19458714]

Rawicz W, Smith BA, McIntosh TJ, Simon SA, Evans E. Elasticity, strength, and water permeability of bilayers that contain raft microdomain-forming lipids. Biophys J. 2008; 94(12):4725–4736. [PubMed: 18339739]

Secomb TW, Skalak R. Surface flow of viscoelastic membranes in viscous fluids. Q J Mech Appl Math. 1982; 35:233–247.

Seifert U, Berndl K, Lipowsky R. Shape transformations of vesicles: phase diagram for spontaneous-curvature and bilayer-coupling models. Phys Rev A. 1991; 44(2):1182. [PubMed: 9906067]

Seifert U, Shillcock J, Nelson P. Role of bilayer tilt difference in equilibrium membrane shapes. Phys Rev Lett. 1996; 77(26):5237–5240. [PubMed: 10062750]

Selinger JV, MacKintosh FC, Schnur JM. Theory of cylindrical tubules and helical ribbons of chiral lipid membranes. Phys Rev E Stat Phys Plasmas Fluids Relat Interdiscip Top. 1996; 53(4):3804–3818.

Steigmann DJ. A model for lipid membranes with tilt and distension based on three-dimensional liquid crystal theory. Int J Nonlinear Mech. 2013 in press.

Steigmann DJ. Fluid films with curvature elasticity. Arch Ration Mech Anal. 1999; 150(2):127–152.

Strandberg E, Esteban-Martin S, Ulrich AS, Salgado J. Hydrophobic mismatch of mobile transmembrane helices: merging theory and experiments. Biochimica Et Biophysica Acta-Biomembranes. 2012; 1818:1242–1249.

Tristram-Nagle S, Zhang R, Suter RM, Worthington CR, Sun WJ, Nagle JF. Measurement of chain tilt angle in fully hydrated bilayers of gel phase lecithins. Biophys J. 1993; 64(4):1097–1109. [PubMed: 8494973]

Virga, E. Variational theories for liquid crystals. Chapman & Hall; London: 1994.

Watkins EB, Miller CE, Majewski J, Kuhl TL. Membrane texture induced by specific protein binding and receptor clustering: active roles for lipids in cellular function. Proc Natl Acad Sci USA. 2011; 108(17):6975–6980. [PubMed: 21474780]

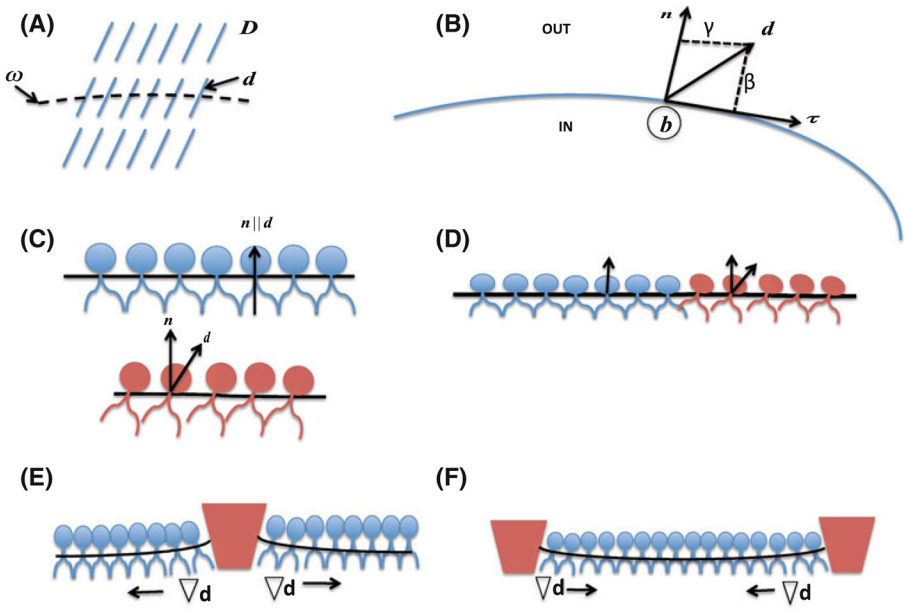

Fig. 1.

The vector fields used to describe the surface. **a** Descent from a 3D director field **D** to a 2D director field **d** restricted to the surface ω. **b** The normal **n**, the tangent τ and the director **d** are shown. The binormal **b** is out of the plane. **c** In the *top panel*, the lipids are aligned along the normal, and in the *bottom panel*, the lipids along the director field. Tilt gradients can arise in several ways, e.g., **d** when two lipids of different resting tilts are adjacent to one another as in a lipid raft or a microdomain, **e** when a protein inserts into one leaflet causing the neighboring lipids to modify their tilt angle so as to minimize their hydrophobic exposure. **f** When two proteins insert themselves at a certain distance from each other, the lipids in between them reorganize their tilt by introducing a tilt gradient

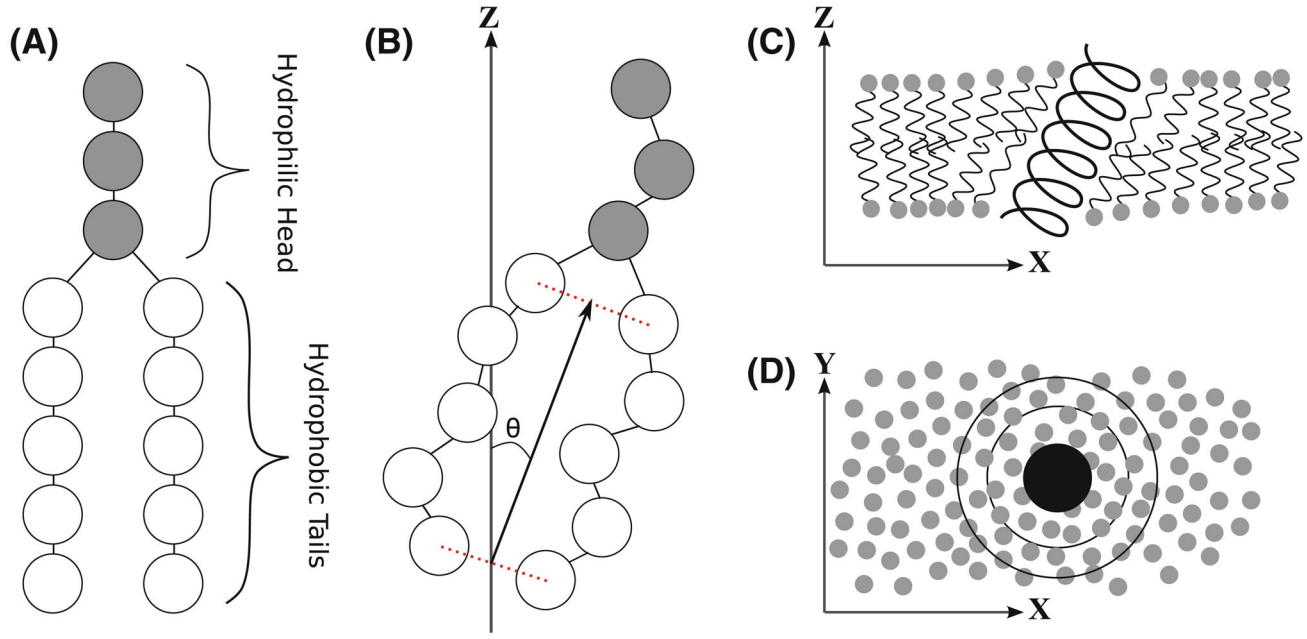

Fig. 2.

Schematic representation of the CG model. **a** A model lipid is represented by equally sized beads. Three hydrophilic beads represent the lipid head group, bonded to two 5-bead hydrophobic tails. **b** The lipid tilt angle, θ, is defined as the angle between the vector connecting the first two tail beads with the last two tail beads and the *Z* direction. A schematic picture of a membrane helix inserted into a bilayer is shown in (**c**). We analyze the tilt angle of lipid around the inserted helix as a function of the radial distance from the helix center, as shown in (**d**). The helix core is represented by a *black circle*, while the lipid head groups are represented by *gray circles*

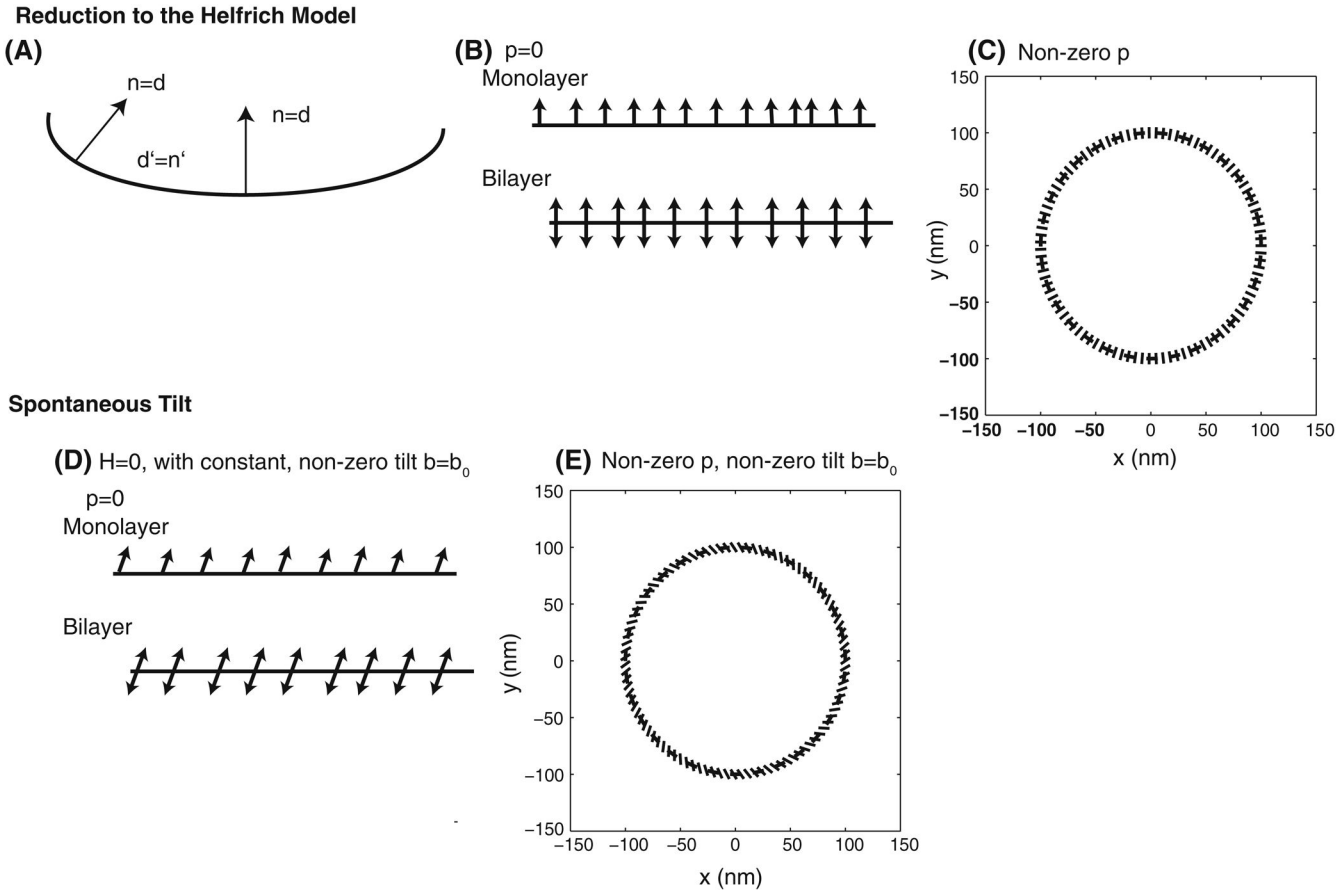

Fig. 3.

Reduction of the tilt model to the Helfrich model. **a** The Helfrich model requires that **d** = **n** and $\mathbf{d}' = \mathbf{n}'$ along the membrane. The value of $\lambda = |\mathbf{r}'(\mathbf{s})|$ is set to 1 in this case. **b** When pressure difference across the membrane $P = 0$, the Helfrich model is limited to describing the cases where the lipids are aligned normal to the membrane. **c** A circular vesicle is a special case of the Helfrich model with zero transverse shear. The size of the vesicle depends on the applied pressure difference across the membrane and the surface tension. The continuum model can also capture spontaneous lipid tilt, where all the lipids have the same, nonzero tilt angle. In (**d**), we show a flat membrane, where the resting tilt is β_0, and **e** when there is a net pressure difference across the membrane, the membrane cross-section is a *circle*, with uniformly tilted lipids

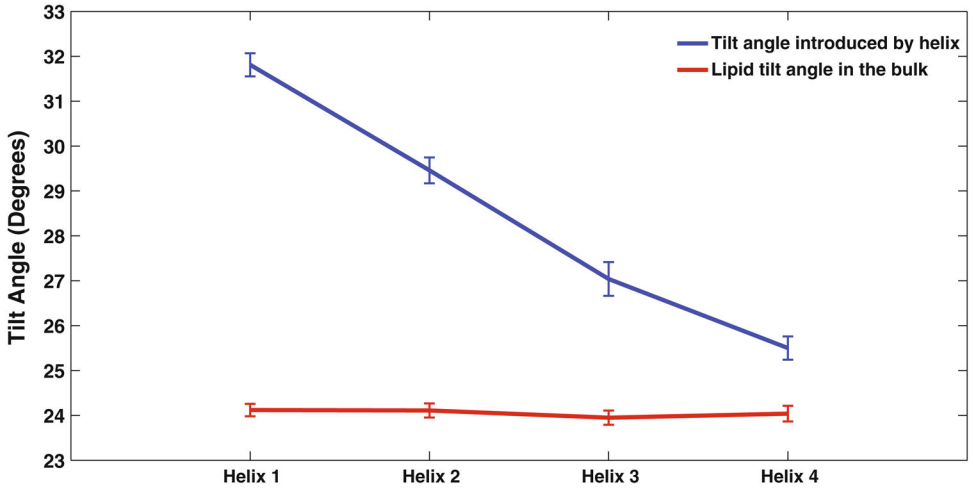

Fig. 4.

Tilt angle introduced by the different helices are shown. In all four cases, the bulk tilt angle of the lipids is the same

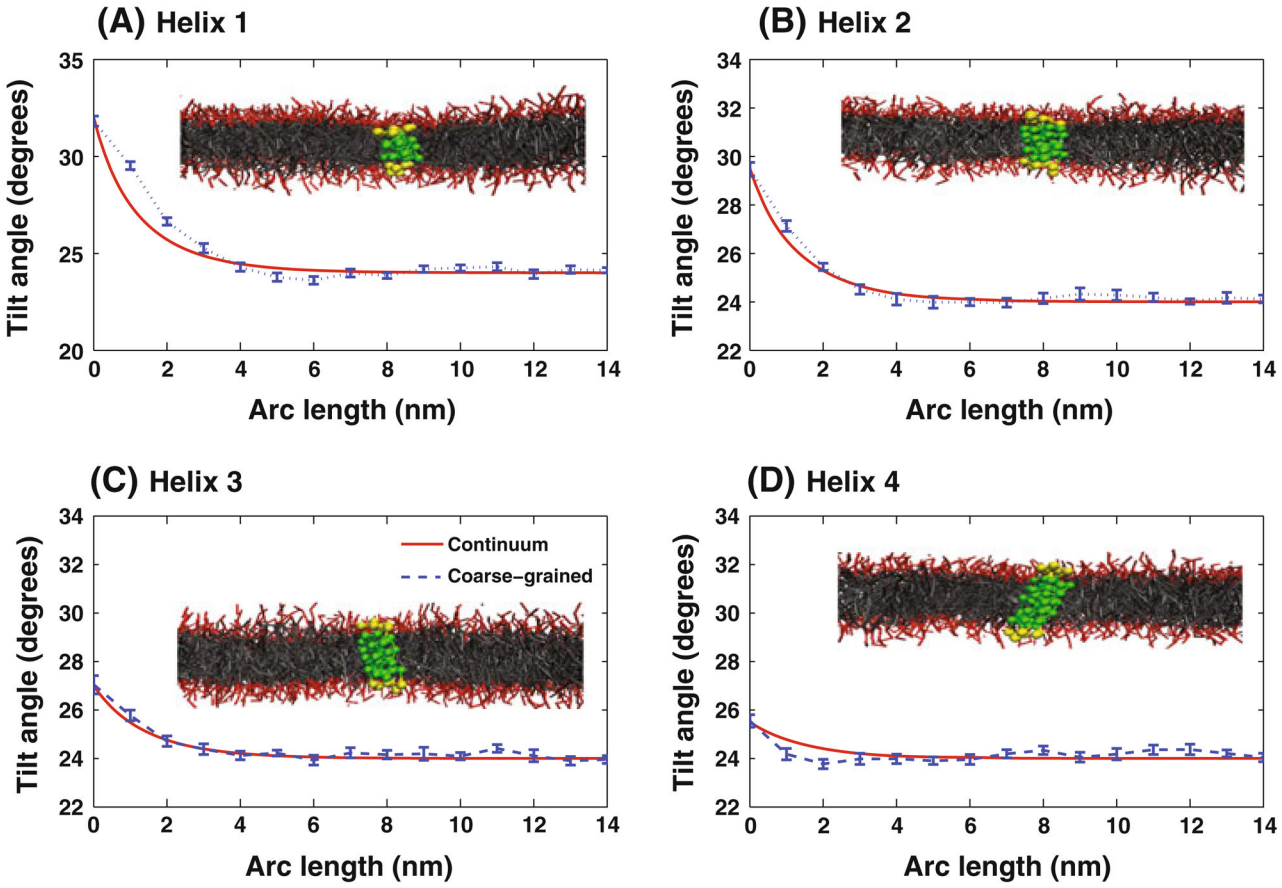

Fig. 5.

Insertion of a hydrophobic protein helix causes the lipids to tilt in the region proximal to the insertion. The graphs show tilt angle comparison between the coarse-grained and continuum models. **a** Helix 1 introduces an 8° change in tilt angle from the bulk. **b** Helix 2 introduces a 5.5° change in tilt angle from the bulk. **c** Helix 3 introduces a 3° change from the bulk, and **d** helix 4 introduces a tilt angle change of 1.5° from the bulk. The continuum model is able to capture the tilt behavior of lipids observed in the coarse-grained model

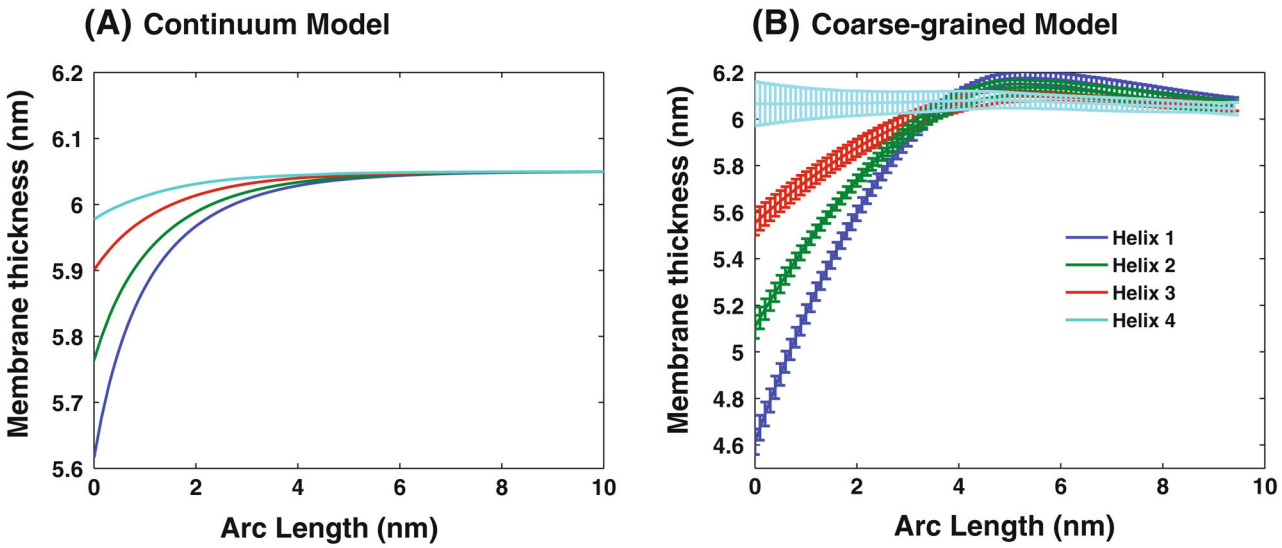

Fig. 6.

Insertion of a protein helix changes the membrane thickness. Increasing protein-induced lipid tilt decreases membrane thickness. **a** Membrane thickness profile in the continuum model and **b** membrane thickness in the coarse-grained model

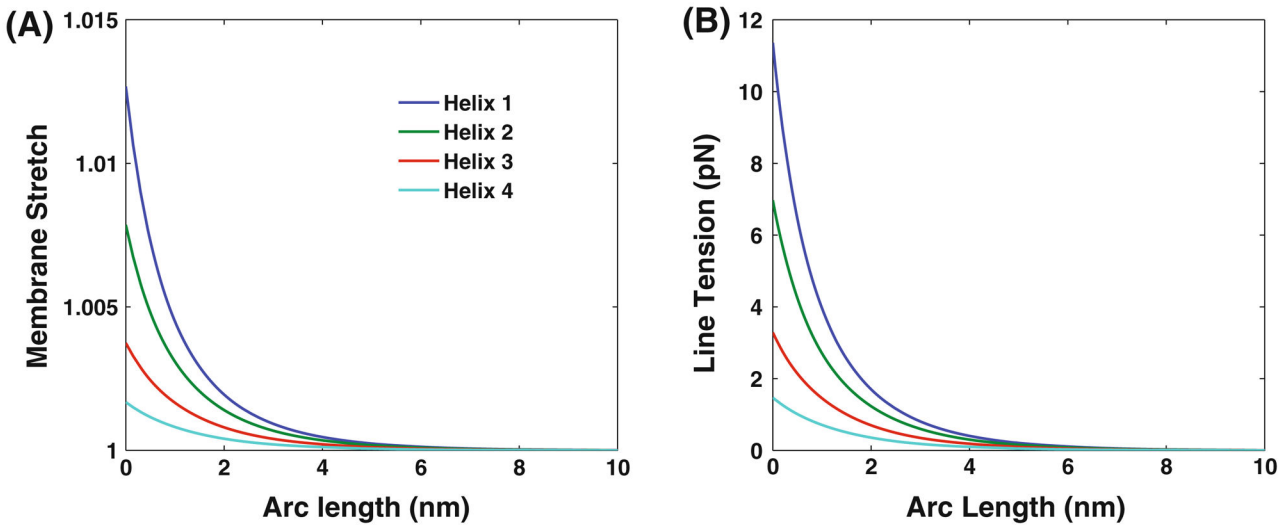

Fig. 7.

Membrane stretch and line tension. **a** Insertion of a protein helix in the membrane causes the membrane to stretch. The membrane stretch increases with the difference in the tilt angle introduced by the protein helix. **b** Line tension, computed as $\Phi_{\mathbf{r}'} \cdot \boldsymbol{\tau}$, is highest near the helix. The line tension increases with increased protein-induced lipid tilt

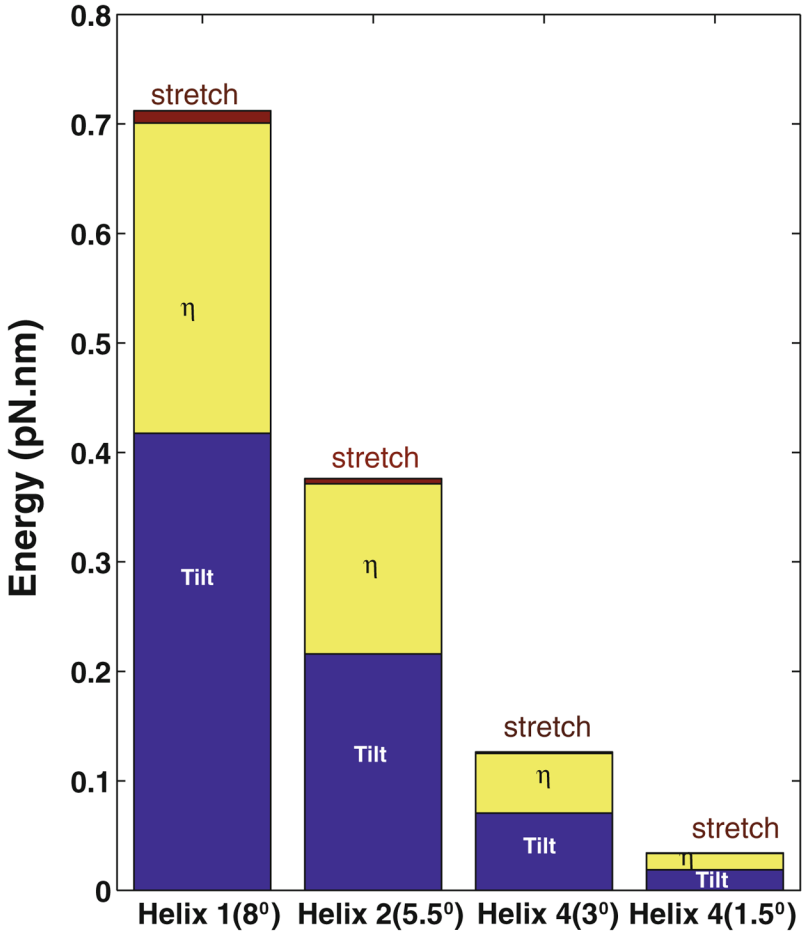

Fig. 8.

The energy penalty on the membrane increases with increasing tilt angle. The number next to the helix name indicates the tilt angle difference from the bulk. Membrane stretch, $k_\lambda(\lambda - 1)^2$, is the least contributor in all four cases. For small tilt angle changes, the contributions from $k_\eta\eta^2$ and $k_\beta(\beta - \beta_0)^2$ are comparable (Helices 3 and 4). As the tilt angle difference increases, the energy contribution from the tilt terms, $k_\beta(\beta - \beta_0)^2$, increases. This tilt contribution is the maximum for Helix 4

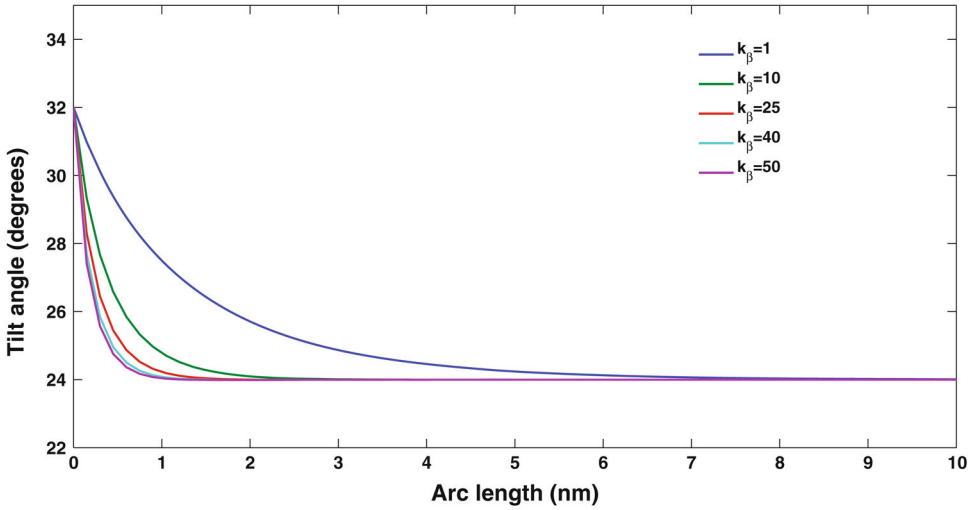

Fig. 9.

Increasing the tilt modulus k_β decreases the tilt relaxation distance. For larger values of k_β, the tilt angle relaxes within 1 nm, which is not in agreement with the observed distribution

Table 1

Notation used in developing the 1D tilt model

Notation	Description	Units
W	Local energy per unit length	pN
s	Arc length in the deformed configuration	nm
S	Arc length in the reference configuration	nm
$\mathbf{r}(S)$	Position vector	
$\mathbf{d}(S)$	Director	nm
$\mathbf{d}'(S)$	Director gradient	dimensionless
$\mathbf{n}$	Normal to the membrane	unit vector
$\boldsymbol{\tau}$	Tangent along the membrane	unit vector
$\beta = \mathbf{d} \cdot \boldsymbol{\tau}$	Tangential component of the director	nm
$\gamma = \mathbf{d} \cdot \mathbf{n}$	Normal component of the director	nm
d_0	Length of the lipid ($d_0^2 = \beta^2 + \gamma^2$)	nm
λ	Local dilation; 1D analog of the two-dimensional areal dilation J	pN
$\eta = \mathbf{d}' \cdot \boldsymbol{\tau} = \beta' - H\gamma$	Tangential component of the director gradient	dimensionless
E	Total energy of the membrane	pN
Ψ	λW, energy in the reference coordinates	pN
α	Lagrange multiplier for lipid length constraint	pN/nm
Φ	Auxiliary function for W including the Lagrange multipliers	pN
P	Pressure difference across the membrane	pN/nm
H	Mean curvature of the membrane	nm^{-1}
σ	Line tension along the membrane, given by $\Phi_{\boldsymbol{\tau}'} \cdot \boldsymbol{\tau}$	pN
k_η	Modulus associated with bending and tilt gradient	pN
k_β	Tilt modulus	$\mathrm{pN/nm}^2$
k_λ	Stretch modulus	pN
k_b	Bending modulus	pN·nm
L	Length of the domain	nm

Table 2

Parameters used in the continuum model

Parameter	Value	Notes	
d_0	6.62255	nm	Measurements from the CG model
k_b	$17k_BT$ = 71.4	pN.nm	Measurements from the CG model
k_η	$k_b/d_0^2=2.856$	Calculated from k_b	
k_β	1	pN/nm^2	Parameter variation; see Fig. 9
k_λ	145	pN	Lipowsky and Sackmann (1995)
β_0	$d_0\cos(24°)$	nm	Measurements of lipid tilt in the bulk from the CG model

Table 3

Non-bonded interaction parameters of the CG model

	w	***h***	***t***	***p***
w	25.0	15.0	80.0	120.0
h	15.0	35.0	80.0	80.0
t	80.0	80.0	25.0	25.0
p	120.0	80.0	25.0	25.0